ISSN 1070-4272, Russian Journal of Applied Chemistry, 2020, Vol. 93, No. 3, pp. 380−392. © Pleiades Publishing, Ltd., 2020.

APPLIED ELECTROCHEMISTRY AND METAL CORROSION PROTECTION

New Ecofriendly Nitrogen-Doped Carbon Quantum Dots as Effective Corrosion Inhibitor for Saturated CO_2 3% NaCl Solution

Jianbo Li[a,b,*], Jie Lv[a,b], Luoping Fu[a,b], Mingjin Tang[c], and Xiaodan Wu[a]

[a] *College of Chemistry and Chemical Engineering, Southwest Petroleum University, Chengdu, Sichuan, 610500 China*
[b] *Oil & Gas Field Applied Chemistry Key Laboratory of Sichuan Province, Southwest Petroleum University, Chengdu, Sichuan, 610500 China*
[c] *College of Chemistry and Chemical Engineering, Sichuan University, Chengdu, Sichuan, 610500 China*
**e-mail:1351456634@qq.com*

Received November 15, 2019; revised January 10, 2020; accepted February 2, 2020

Abstract—Inspired by the high-water solubility, photoluminescence and low cytotoxicity of N-doped carbon quantum dots (N-CQDs), fluorescent corrosion inhibitors with size of 4–8 nm were synthesized from disodium ethylenediaminetetraacetate, sulfamic acid, and urotropine salt. We expect that these N-CQDs may possess an excellent protective ability to inhibit the corrosion of carbon steel in aggressive solutions owing to its special functional group. The inhibitory mechanism of the inhibitor on N80 steel in saturated CO_2 3 wt % NaCl solution was studied by weight loss, adsorption curve fitting, electrochemical measurement, and surface morphology and elemental analysis. The results show that corrosion of N80 carbon steel in saturated CO_2 3 wt % NaCl solution is significantly inhibited by the addition of N-CQDs, which is attributed to the formation of its adsorption film, preventing the contact of iron with chloride ions and is an effective corrosion inhibitor.

Keywords: N 80 carbon steel, N-doped carbon quantum dots, electrochemical, corrosion inhibitor

DOI: 10.1134/S10704272200300106

INTRODUCTION

Mild steels are very common and widely used metallic material due to low cost and good mechanical properties [1, 2], they are wildly used in boilers, oil pipelines and mechanical storage components [3–5]. In the oil and gas field mining process, especially in the middle and late stage of the mining phase, it is often necessary to add CO_2 flooding to increase oil and gas production. However, the injected CO_2 is dissolved in the oilfield water, and the action of Cl^- and dissolved oxygen in the formation makes the corrosion of the mild steel quite serious. Corrosion of mild steel in CO_2 brine environment has been studied extensively [6–10].

In order to prevent corrosion of the pipeline by CO_2 saline solution, the most economical and effective method is to add a corrosion inhibitor to the pipeline. Corrosion inhibitors mainly contain hetero atomic

compounds such as N, O, P, S, which are adsorbed on the metal surface by non-bonded electrons (orphaned electrons) and π electrons in the molecule, thereby reducing the contact area between corrosive medium and the metal surface, and slowing down the corrosion. At present, a large number of CO_2 saline solution corrosion inhibitors, such as imidazoline derivatives, amides, Schiff bases, and quaternary ammonium salts, have been reported [11–13]. With the improvement of people's health awareness, green chemistry has also received more and more attention. However, these organic compounds are complicated to synthesize, expensive, and difficult to degrade naturally, so they are also greatly challenged in legal policy. Development of environment-friendly corrosion inhibitors has become a research hotspot at current period.

Carbon quantum dots (CQDs), which are a new class of fluorescent carbon nanoparticles, have become increasingly noteworthy because of their high and stable fluorescence, low toxicity, substantial biocompatibility, good water solubility, and stable chemical properties. All of these unique and superior properties make them suitable for use in biosensing, medical imaging, drug detection, photocatalysis, and other biological sciences. To date, numerous researchers have successfully synthesized CQDs by laser ablation, microwave radiation, and hydrothermal methods [14–19]. Very recently, both experimental and theoretical results confirmed that heteroatom doping was an effective method to improve the electronic and optical properties of CQDs. Teng et al., reported a dexterous microwave-assisted method to synthesize N and S co-doped CQDs (N,S-CQDs) for improving photoluminescence yield [20–25]. By Yang et al. [26] green and low-cost aquatic plant ECs were used to produce blue fluorescent N-CQDs by hydrothermal method, facilitating the assemble process for many optoelectronic devices, such as the solar cells, which can yield the solar-to- electrical conversion efficiency of 0.17% [26].

At present, the anti-corrosive applications of carbon nanomaterials, such as super-hydrophobic materials, are mostly devoted to hydrophobic coating [27–29], there are few reports on the use of CQDs as a corrosion inhibitor in the field of corrosion protection. By Cui et al., carbon quantum dots were prepared using amino salicylic acid (ASA) as a precursor. These materials were found to have a unique structure and effectively inhibit the corrosion of carbon steel in 1 M HCl solution [30]. The surface of the carbon quantum dots contains a large number of reactive groups, such as hydroxyl group, carboxyl group, etc. So, doping the N-containing atom causes it to form a coordination compound with the outer layer of the iron (*d* orbital), thereby adsorbing strongly on the surface of the carbon steel. With the strong electronegativity and electron-donating capability of N atoms, N-CQDs were anticipated as an effective corrosion inhibitor.

We reported the synthesis of N-doped carbon quantum dots by microwave irradiation in 3 min, which can effectively inhibit the corrosion of mild steel in CO_2-saturated 3% NaCl solution. The structure and spectral characteristics of N-CQDS were analyzed by Fourier transform infrared spectroscopy (FTIR), X-ray diffraction (XRD), Raman spectroscopy (Raman), ultraviolet-visible spectroscopy (UV-vis), fluorescence spectrophotometer (PL), X-ray photoelectron spectroscopy (XPS) and transmission electron microscopy (TEM). Static weightlessness method, electrochemical measurements were used to study the inhibition effect and mechanism of N-CQDs. The surface morphology of carbon steel is measured by scanning electron microscopy (SEM) and energy dispersive spectroscopy (EDS).

EXPERIMENTAL

Material and Specimen Preparation

In this study, disodium ethylenediaminetetraacetate (EDTA), sulfamic acid and urotropine were purchased from Aladdin (Shanghai, China). N80 carbon steel samples were used as substrates. The elemental composition of carbon steel is as follows: C (≤0.20), Si (≤0.35), Mn(≤1.4), P (≤0.045), S (≤0.045), Cr (≤0.3), Ni (≤0.3), Cu (≤0.3), and Fe (remainder). The samples were then ground with 200, 400, 600, 800, and 1200 grade silicon carbide sandpaper, and then cleaned with ethanol and degreased with acetone in turn.

The steel sheet is dried with nitrogen gas and then immersed in CO_2-saturated 3% NaCl solution corrosive medium. Deionized water and analytical NaCl reagent were used to prepare 3% NaCl test solution, which was saturated and filled with 99% CO_2 gas for 6 h. Deionized water was used during whole experiments.

Synthesis of N-CQDs

N-CQDs were synthesized by microwave treatment of EDTA, sulfamic acid, and urotropine as raw materials. Among them, EDTA (3.38 g) was used as carbon source, sulfamic acid (1.94 g), and urotropine (1.4 g) as precursors, which are ultrasonically dissolved in deionized water. Then, the mixture was transferred to a PTFE reactor. The PTFE reactor was placed in a microwave oven with a power setting of 700 W, and the reaction time was about 3 min. The reactor was taken out when it cooled to 25°C. Next step, the mixture in reactor was transferred to a centrifuge tube, and centrifuged in a 4000 rpm for 30 min to obtain a crude product. The crude product was through a filter paper, and then the 0.22 μm microporous membrane was used to remove large particles. Thereafter, the solution was purified against deionized water by using a dialysis membrane with 1000 pore size for 24 h to remove the incompletely reacted small molecule. Finally, rotary evaporation and

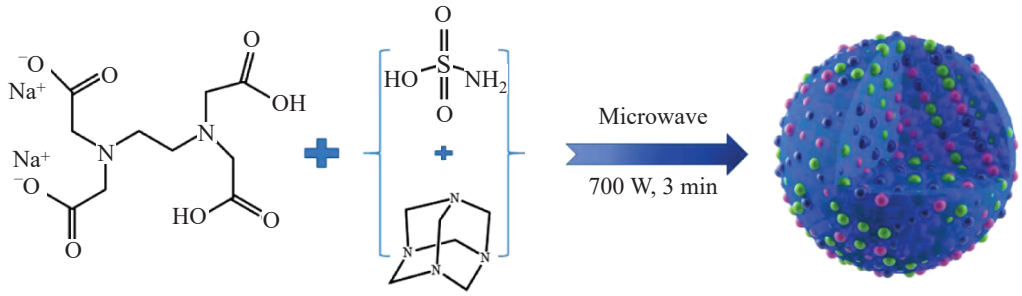

Fig. 1. Schematic illustration for the synthesis process of N-CQDs.

freeze-drying were carried out to obtain pure N-CQDs. The schematic diagram of synthesis is shown in Fig. 1.

Preparation of Electrode and Solutions

The N 80 carbon steel electrode substrate was ground with silicon carbide sandpaper of 200, 400, 600, 800, and 1200 grade respectively, the exposed area of the electrode is 1 cm^2. Then, it was successively washed with pure water, ethanol and acetone, and finally dried with nitrogen gas. The CO_2-saturated 3% NaCl solution in the absence and presence of various concentrations of N-CQDs (50, 100, 200 400, and 600 mg L^{-1}) was prepared from deionized water.

Characterization of N-CQDs

The Nicolet 6700 (WQF 520, China) infrared spectrometer was employed to characterize the N-CQDs structure. The UV–vis results were measured on UV-3600 (Shimadzu, Japan) and the photoluminescence emission spectra were recorded by fluorescence spectrophotometry (PerKinEImer LS55 American). The structure of N-CQDs was characterized by XRD (Cu-target K_α Ray, λ = 0.15406 nm, scanning range of 10°–70° X Pert PRO MPD，Netherlands). The Raman spectrum and XPS were acquired by LabRAM HR800 (Horiba JobinYvon), Thermo ESCALAB 250XI, respectively. SEM and EDS analysis was conducted with ZEISS EV0 MA15 (Germany). The TEM images were acquired from TF20, Jeol 2100F (Japan), which is used to characterize its size and morphology distribution.

Weight Loss Measurements

The suspended N80 steel test piece (40.00 mm × 13.00 mm × 1.70 mm: length, width, height) was ground with SiC sandpaper of different particle sizes to give the surface a uniform metallic luster. It was then washed with ethanol, degreased with acetone, dried with nitrogen, kept in a desiccator, and weighed to the nearest 0.1 mg.

Then the test piece was immersed in a bottle containing 500 mL of CO_2-saturated 3% NaCl solution with and without inhibitors at 70°C for 72 h. The solution was bubbled with CO_2 gas continuously throughout experiments.

After the tests, the test piece was taken out, thoroughly rinsed with distilled water, dried, and accurately weighed. Each set of experiments was repeated three times to ensure reproducibility.

The corrosion rate and corrosion inhibition efficiency of the test piece can be calculated by the following formula:

$$v_{coor} = \frac{8.76\times10^4\,\Delta m}{St\rho}, \quad (1)$$

where v_{coor}, Δm , ρ, S, and t are the corrosion rate (mm/A), weight loss (g), test sample density (g/cm^3), exposed sample area (cm^2), and immersion time (h), respectively. Subsequently, the inhibition efficiency (η, %) of the N-CQDs inhibitor was calculated by:

$$\eta = \frac{v^0_{coor} - v_{coor}}{v^0_{coor}}\times100, \quad (2)$$

where v^0_{coor} and v_{coor} are the corrosion rates in the absence and presence of inhibitors, respectively.

Surface Analysis

In order to measure the surface roughness of N80 carbon steel sample after 72 h of immersion in CO_2-saturated 3% NaCl solution in the absence and presence of 600 mg L^{-1} of N-CQDs, scanning electron microscopy was employed and energy dispersive spectroscopy were used to analyze morphological features and element composition of carbon steel surface.

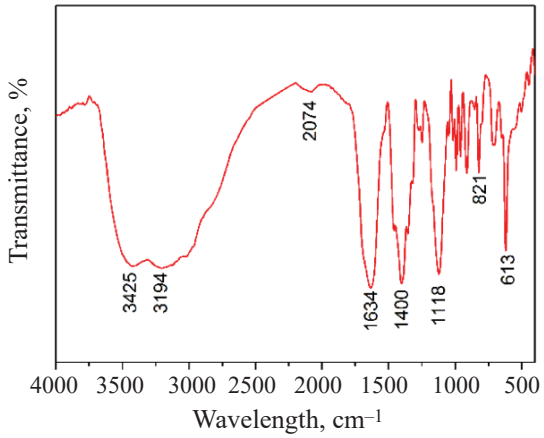

Fig. 2. IR spectrum of N-CQDs.

Electrochemical Studies

All electrochemical measurements were carried out using CHI650 electrochemistry workstation. The potentiodynamic polarization and electrochemical impedance spectroscopy (EIS) of N-CQDs were analyzed by conventional three-electrode system, a platinum foil was used as a counter electrode, a saturated calomel electrode (SCE) was used as a reference electrode, and carbon steel served as a work electrode (WE), obtaining the polarization curves and EIS data of N80 carbon steel. The entire experimental process was carried out at a stable open circuit potential, and the test temperature was 25°C. EIS measurements were performed at E_{corr} over the frequency range of 10^5 Hz to 0.01 Hz with perturbation amplitude of 5 mV. EIS data were analyzed by ZView software, potentiodynamic polarization curves were measured at scanning rate of 1 mV/s from –250 to 250 mV, and the relationship between current density and corrosion potential was obtained, according to the relevant theory of electrochemistry, the corrosion inhibition rate (η, %) of the corrosion process can be calculated by Eq. (3).

$$\eta = \frac{I^0_{coor} - I_{coor}}{I^0_{coor}} \times 100, \quad (3)$$

where I^0_{coor} and I_{coor} are the corrosion current values of carbon steel immersed in test solution without and with inhibitors, respectively.

The impedance parameters obtained from the EIS can also be used to calculate the suppression efficiency (η) after fitting with the ZView software, the calculation formula is as follows:

$$\eta = \frac{R_t - R^0_t}{R_t} \times 100, \quad (4)$$

where R_t and R_t^0 are charge transfer resistors in the absence and presence of inhibitors, respectively.

RESULT AND DISCUSSION

Characterization of N-CQDs

The IR spectrum of N-CQDs is shown in Fig. 2. The spectrum for N-CQDs possessed various absorption bands, the broad absorption peaks at 3425 cm^{-1} composed by O–H and N–H, and the peaks at around 3194 cm^{-1} were attributed to the C–H bond, the peak at 2074 cm^{-1} was typical absorption for cumulated double bonds attributed to N=C=S, N=C=O or S=C=O, the peak at 1634 cm^{-1} indicates the characteristic absorption peak of the amide group stretching vibration, the peak at 1400 cm^{-1} is attributed to the tensile vibration of the C–N or C–S bond, the peak at 1118 cm^{-1} indicate the existence of $–SO_3$, 821 and 613 cm^{-1} belong to C–O bond telescopic vibration and C–C bond skeleton vibration, respectively.

It can be seen from Fig. 3 that N-CQDs can be observed at different resolutions with similar spherical structure with good dispersion and diameter between 4

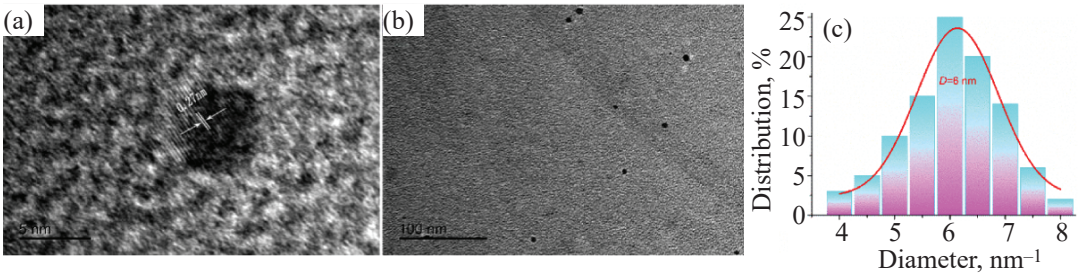

Fig. 3. The characterization of N-CQDs for (a) TEM image, (b) HRTEM image, (c) particle size distribution image.

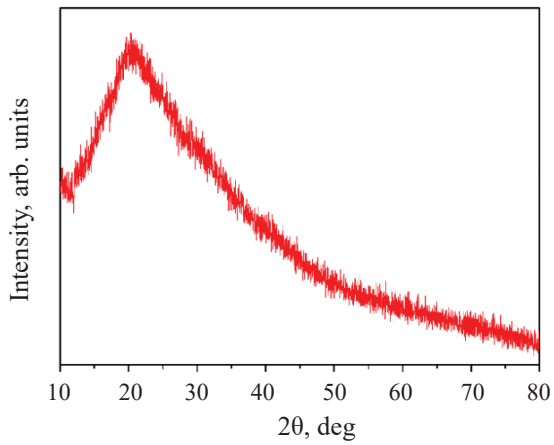

Fig. 4. (Color online) XRD diagram of N-CQDs.

and 8 nm. High-resolution TEM clearly revealed that the synthetic N-CQDs show noticeable lattice fringes with interplanar distance of around 0.27 nm, showing a high-crystalline structure, is typical graphite phase (020) crystal plane.

The XRD diagram of N-CQDs (Fig. 4) presented a broad diffraction peak centered at 2θ of approximately 20.2°, as can be seen from the XRD peak shape, the synthesized N-CQDs are amorphous, and no continuous and complete crystal structure. With the corresponding interlayer spacing of around 0.405 nm, compared with the graphite 002 crystal plane (0.34 nm), N-CQDs have a wider interplanar spacing, which may be caused by the doping of hetero atoms such as N, which increases the repulsive force between the molecules.

Figure 5 shows UV-vis and fluorescence spectra of N-CQDs, the UV–vis absorption spectrum contains two apparent absorption bands, influenced by double bond, conjugate and solitary electron, the absorption bands at 240 and 368 nm belong to the C=O bond π-π* electron transition and the C=N bond *n*-π* electron transition, respectively. From the fluorescence spectra of N-CQDs, the fluorescence intensity increases first and then decreases with the increase in excitation wavelength, which illustrates the ordinary excitation-dependent emission behaviors of N-CQDs, and the maximum fluorescence intensity of N-CQDs was obtained when the excitation wavelength was 350 nm, with the corresponding emission wavelength is 425 nm. The emission point corresponding to a certain excitation wavelength depends on the surface state of N-CQDs, the reason for its luminescence is generally considered to be a surface defect formed by the oxidation of the surface of N-CQDs, the trapping of excited energy from the passivated surface on heteroatom resulted in the absorption, which may contribute to the strong fluorescence.

For the sake of the analysis on different state of carbon, the Raman spectra of N-CQDs (Fig. 6) was acquired using 532 nm laser, the peaks at 613, 915, and 972 cm^{-1} are assigned to ring –N stretching mode, ring–CH wagging mode, and CH in plane bending, the peak at 1310 cm^{-1} is assigned to the C–$N^{\bullet+}$ stretching modes of delocalized polaronic charge carriers revealing that N-CQDs is in the doped state. The peak at 1416 cm^{-1} (D-band) is attributed to sp^3 hybrid carbon atoms of amorphous structure, which is caused by graphite defect, while the peak at 1665 cm^{-1}(G-band) is assigned to the vibration of sp^2 hybrid carbon atoms in a two-dimensional hexagonal structure [31]. The

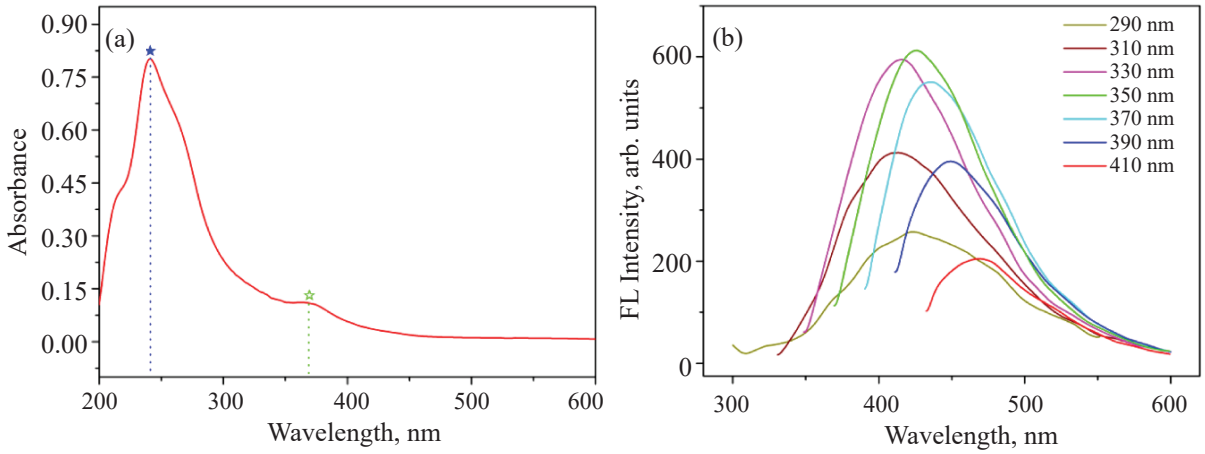

Fig. 5. (Color online) (a) UV–vis absorption spectra, (b) FL emission spectra at different excitation wavelengths.

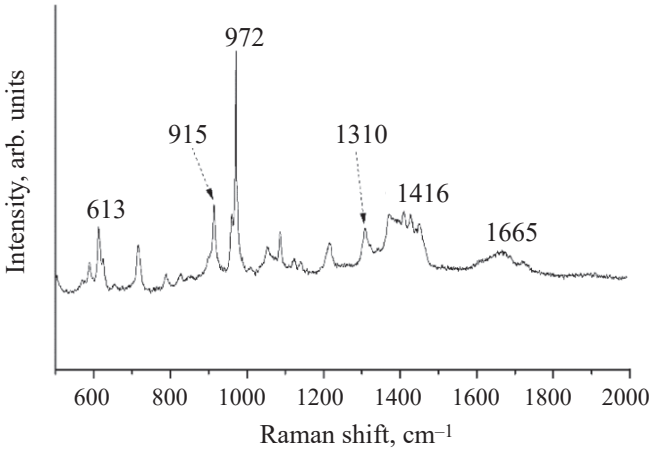

Fig. 6. Raman spectra of N-CQDs.

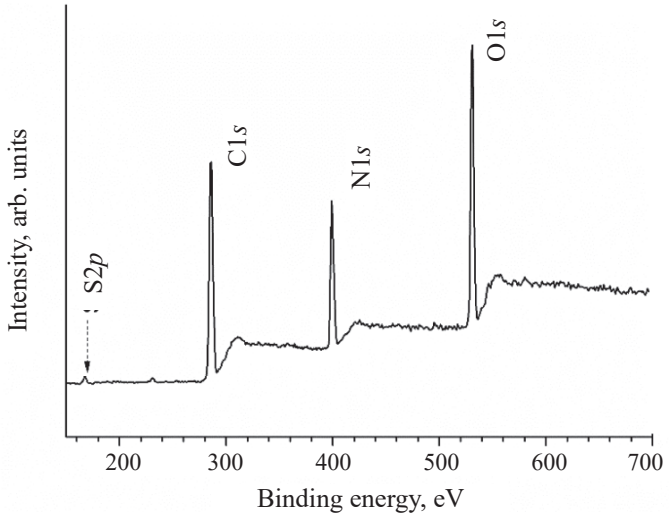

Fig. 7. XPS survey scans of N-CQDs.

ratio of D band to G band (ID/IG) reflects the degree of graphitization of carbon materials, its value is 0.85.

The chemical composition was characterized by XPS spectroscopy. The full-range XPS spectrum of the synthesized N-CQDS is shown in Fig. 7, the relative content of each atom of N-CQDs can be seen from Table 1. Figure 8 shows the C1*s*, N1*s*, O1*s*, and S2*p* in high-resolution XPS spectra. The C1*s* spectra of N-CQDs (Fig. 8a) display three peaks at 284.5, 285.5, and 287.2 eV, which are attributed to C=C, C–N/C–N, and C=O/C–S, respectively [25]. Figure 8b shows the N1*s* peak, two of the component peaks were assigned to pyridine N (398.3 eV) and pyrrole N (400.4 eV) [31]. The O1*s* spectrum (Fig. 8c), can be divided into peaks at 531.5 and 532.8 eV, which are attributed C=O and C–OH/C–O–C bonds. Two peaks at 164.1 and 165.5 eV ascribed to C=S/C–S and CH_3S=O, respectively, appeared in the $S_2p^{3/2}$ spectrum (Fig. 8d). These results

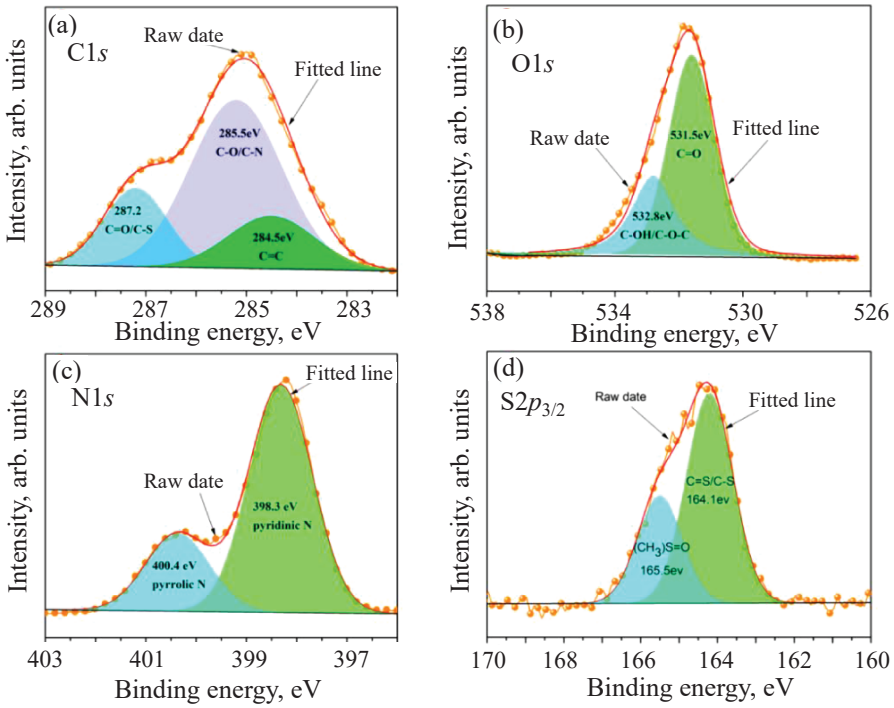

Fig. 8. (Color online) High-resolution XPS spectra of N-CQDs.

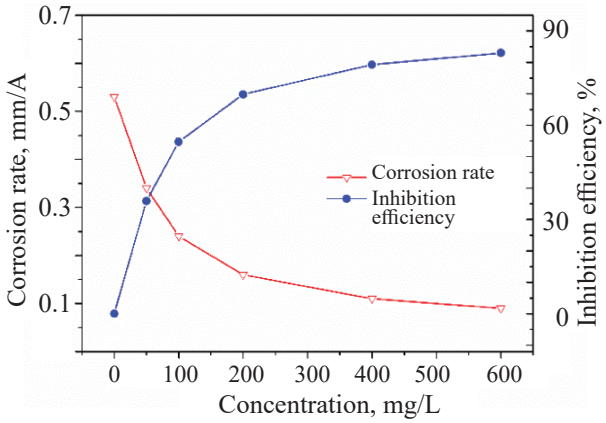

Fig 9. (Color online) The variation of the corrosion rate and inhibition efficiency in the presence of various concentrations of N-CQDs.

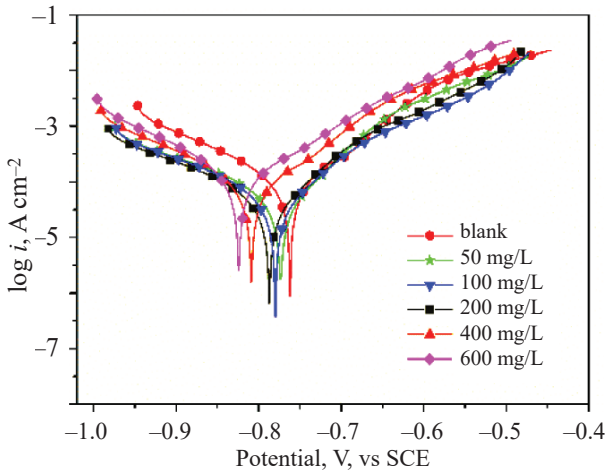

Fig. 10. (Color online) Potentiodynamic polarization curves of N80 carbon steel in CO_2-saturated 3% NaCl solution in the absence and presence of different concentrations of N-CQDs.

indicate that N-doped carbon quantum dots (N-CQDs) have been successfully synthesized.

Weight Loss Measurements

From Fig. 9, it can be seen that the corrosion rate of carbon steel in N-CQDs is lower than that in blank solution at 70°C, and the corrosion inhibition effect is obviously improved with the increase of N-CQDs concentration. When the amount of corrosion inhibitor is 600 mg/L, the N-CQDs corrosion efficiency is 83.7%.

Table 1. The relative contents of C, N, O and S atoms for N-CQDs

	C, at. %	N, at. %	O, at. %	S, at. %
N-CQDs	55.81	19.84	23.4	0.95

Obviously, adding N-CQDs can reduce the corrosion rate of carbon steel.

Electrochemical Measurements

Potentiodynamic polarization measurement. Potentiodynamic polarization curve can be used to analyze the properties and influencing factors of corrosion process [37–39]. Potentiodynamic polarization curves of N80 carbon steel in CO_2-saturated 3% NaCl solution with various concentrations of N-CQDs is given in Fig. 10. The values of corrosion current density (i_{corr}), corrosion potential (E_{corr}), cathodic and anodic Tafel slopes (β_c and β_a), as well as the corrosion inhibition efficiency (η) as a function of concentrations of N-CQDs is summarized in Table 2.

From the visual examination of polarization curves in Fig. 10, with the addition of N-CQDs, there is no obvious

Table 2. Electrochemical parameters obtained from potentiodynamic polarization curves of N80 carbon steel in CO_2-saturated 3% NaCl solution in the absence and presence of different concentrations of N-CQDs

ρ, mg L^{-1}	E, mV	β_a, mV/dec	β_c, mV/dec	I, μA cm^2	η, %
blank	–762	101.50	141.70	310.0	/
50	–773	99.61	184.08	177.6	42.7
100	–779	116.53	180.65	135.8	56.2
200	–786	111.85	143.28	107.6	65.3
400	–810	125.88	184.88	86.5	72.1
600	–824	130.92	135.06	50.5	83.7

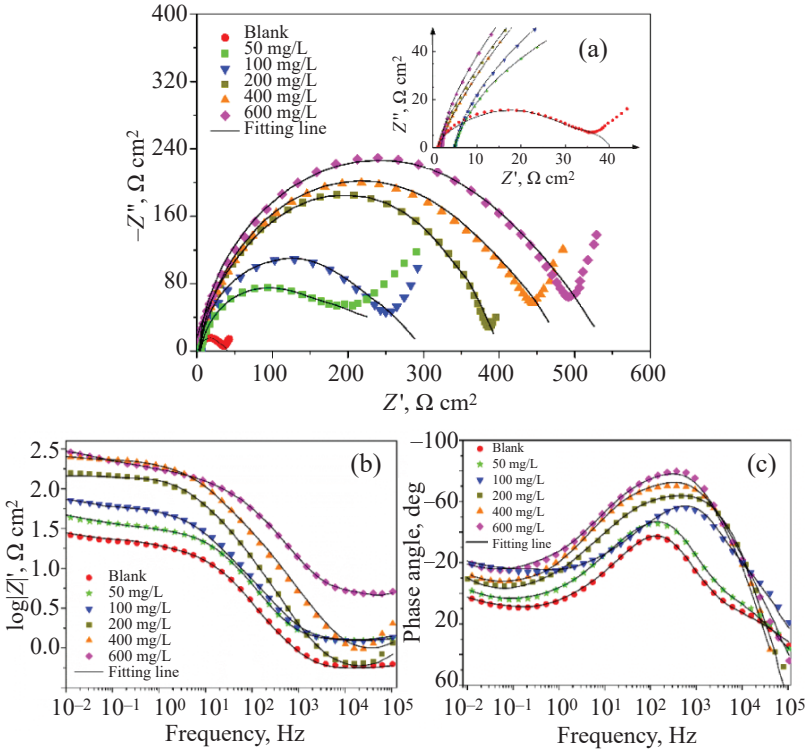

Fig. 11. (Color online) Nyquist and bode plots of N80 carbon steel in CO_2-saturated 3% NaCl solution in the absence and presence of different concentrations of N-CQDs.

change in the Tafel curve of the cathode and anode reactions, which indicates that N-CQDs does not change the reaction mechanism of the anode dissolution process and the cathode dissolved oxygen process, compared with the blank group, the self-corrosion potential tends to shift to the cathode as a whole. According to Table 2, the change value of corrosion potential is 62 mV. it is generally considered to be less than 85 mV as a hybrid corrosion inhibitor, therefore, N-CQDs is considered to be a mixed corrosion inhibitor which mainly inhibits cathode. The change of β_c is obviously higher than β_c, which further proves that N-CQDs mainly inhibits the hydrogen evolution kinetics of carbon steel cathode surface [40-41]. The results show that N-CQDs can be used as a good corrosion inhibitor for CO_2-saturated 3% NaCl solution.

Electrochemical impedance spectroscopy measurement. As shown in Fig. 11, Nyquist diagram shows that the impedance is warburg impedance, and the approximate half-arc diameter in the first half reflects the difficulty of charge transfer on the electrode surface. Obviously, with the addition of N-CQDs, the interface impedance becomes larger, carbon steel Corrosion resistance increases; the latter half is a low frequency induction loop, the formation of which is attributed to the relaxation process on the metal plate, like on the metal substrate (Fig. 11a) [41]. Further, it can be clearly seen from the Bode diagram that the addition of N-CQDs leads to the increase of impedance modulus, this can be attributed to the protective film formed on the surface of steel by N-CQDs (Fig. 11b). There is only one extreme value in the phase diagram. The corrosion process of the surface metal solution has only one time constant. With the addition of N-CQDs, the peak height increases accordingly, which means that the inhibitor molecules are adsorbed on the surface of the carbon steel, and the capacitance at the interface of the metal solution in the response is larger (Fig. 11c) [42].

To better fit the parameters of impedance spectra, an equivalent circuit is proposed to analyze the corrosion mechanism of N80 carbon steel in CO_2-saturated 3% NaCl solution (Fig. 12). These circuits are measured at different concentrations of N-CQDs. In Fig. 12, R_s is solution resistance, Q is composed of membrane capacitance C_f and dispersion index n, R_2 is membrane resistance, C_{dl} is double-layer capacitance, and R_{ct} is charge transfer resistance [43–45]. The corresponding values are listed in Table 3. After adding N-CQDs, the

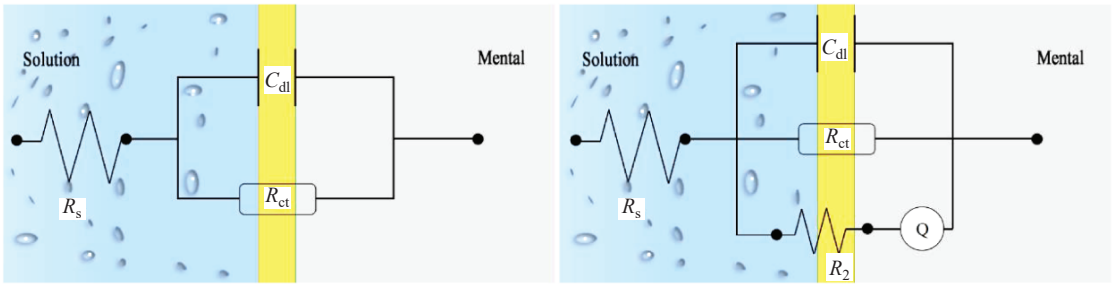

Fig. 12. (Color online) Equivalent circuit analog diagram.

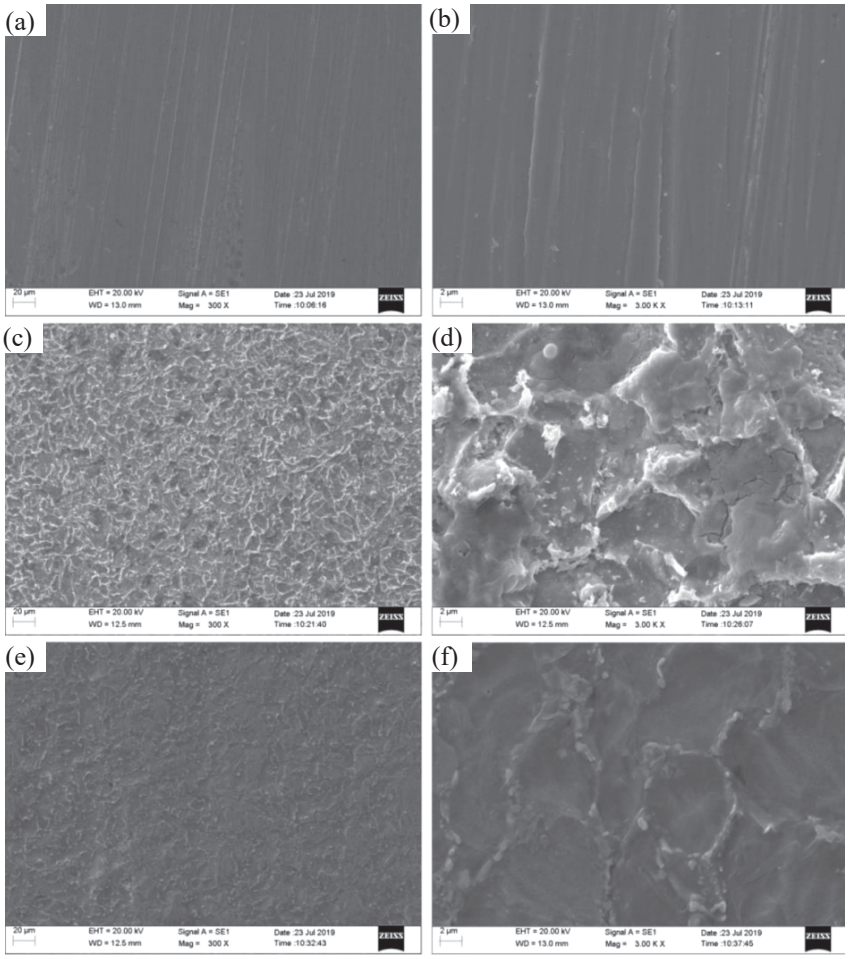

Fig. 13. (Color online) SEM image of (a, b) polished N80 carbon steel and immersed in saturated CO_2 3% NaCl solution for 72 h (c, d) in the absence and (e, f) presence of 600 mg/L N-CQD.

membrane capacitance (C_f) was significantly lower than the blank group, mainly because N-CQDs could form a protective adsorption film on the surface of N80 carbon steel, which prevents the diffusion of dissolved oxygen to the electrode surface and the reduction of dissolved oxygen on the electrode surface. At the same time, the double-layer capacitance (C_{dl}) is also lower than the blank solution. This is due to the adsorption of N-CQDs at the carbon steel/solution interface, so that the water molecules with larger interfacial dielectric constants are gradually replaced by larger corrosion inhibitor molecules with smaller dielectric constant, thereby, the dielectric constant of the interface is changed, and (C_{dl}) becomes small. As the concentration of N-CQDs

Table 3. Fitting parameters obtained from EIS results of N80 carbon steel in CO_2-saturated 3% NaCl solution in the absence and presence of different concentrations of N-CQDs

ρ_{inh}, mg L^{-1}	R_s, Ω cm^2	C_f, μF cm^{-2}	n	C_{dl}, 10^{-5} F cm^{-2}	R_2	R_{ct}, cm^2	η, %
Blank	1.32	/	/	22.31	/	33.95	/
50	0.98	3.32	0.78	7.92	8.74	58.03	41.5
100	1.5	2.73	0.57	6.73	19.26	74.29	54.3
200	0.81	2.89	0.54	5.86	29.31	92.76	63.4
400	1.46	3.98	0.55	6.44	33.01	110.23	69.2
600	0.84	2.31	0.61	5.81	24.65	165.6	79.5

increases, R_{ct} also increases significantly, and the purpose of slowing down the corrosion of carbon steel is achieved by suppressing charge transfer [46–48].

SEM Analysis

SEM images of the N80 carbon steel before and after 72 h of immersion in saturated CO_2 3% NaCl solution in the absence and presence of 600 mg/L of N-CQDs is also obtained, As shown in Figs. 13a, 13b the polished N80 carbon steel is relatively smooth with some polished scratches. Figures 13c, 13d illustrate the surface morphology without adding N-CQDs, it can be seen that the surface of the steel carbon is rough and there are some cracks and pits, and there are many corrosion products. The surface of the steel sheet in Figs. 13e, 13f is relatively smooth, and pitting corrosion is significantly reduced. This may be related to the adsorption of N-CQDs on the surface of carbon steel, which prevents the direct reaction of external ions on the metal surface, thus achieving the purpose of reducing corrosion.

The distribution of elements adsorbed on the surface of carbon steel was characterized by high- resolution SEM, the N80 carbon steel after 72 h of immersion in saturated CO_2 3% NaCl solution in the (b) absence and (a) presence of 600 mg/L of N-CQDs. It can be clearly seen that by adding a corrosion inhibitor, according to Fig. 14, new N and S elements are adsorbed on the surface of carbon steel, which further proves that N-CQDs can be well adsorbed on the surface of carbon steel.

EDS Analysis

After 72 h of immersion in saturated CO_2 3% NaCl solution without and with 600 mg/L N-CQDs, the

EDS spectra and corresponding percentage atomic contents are displayed in Fig. 15. It can be seen from Fig. 15a that the surface of the newly polished carbon steel mainly consists of C, O, Si and Fe. Comparing Fig. 15b with Fig. 15c, it can be found that N and S peaks appear newly in the EDS spectra of the carbon steel sheet soaked with N-CQDs, and the peak intensity of Cl is significantly reduced, because the corrosion inhibitor adsorbs on the carbon steel, preventing the reaction of carbon steel with solution.

To directly compare the variation on the surface composition, the graph of the variation of content for different elements (Fig. 15d) demonstrates that the percentage

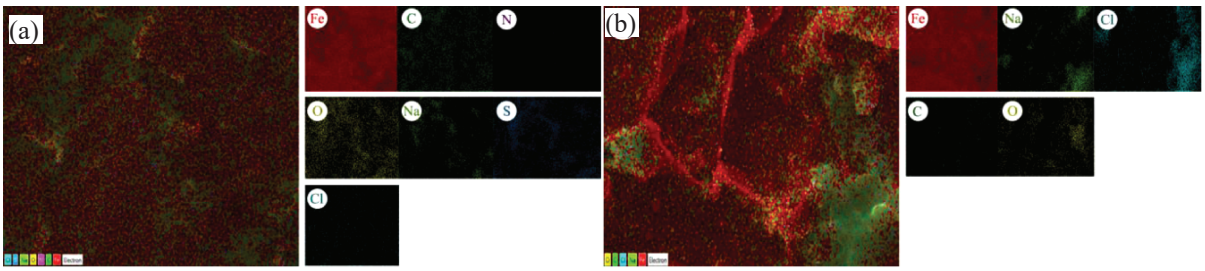

Fig. 14. (Color online) High-resolution SEM images of N80 carbon steel element distribution.

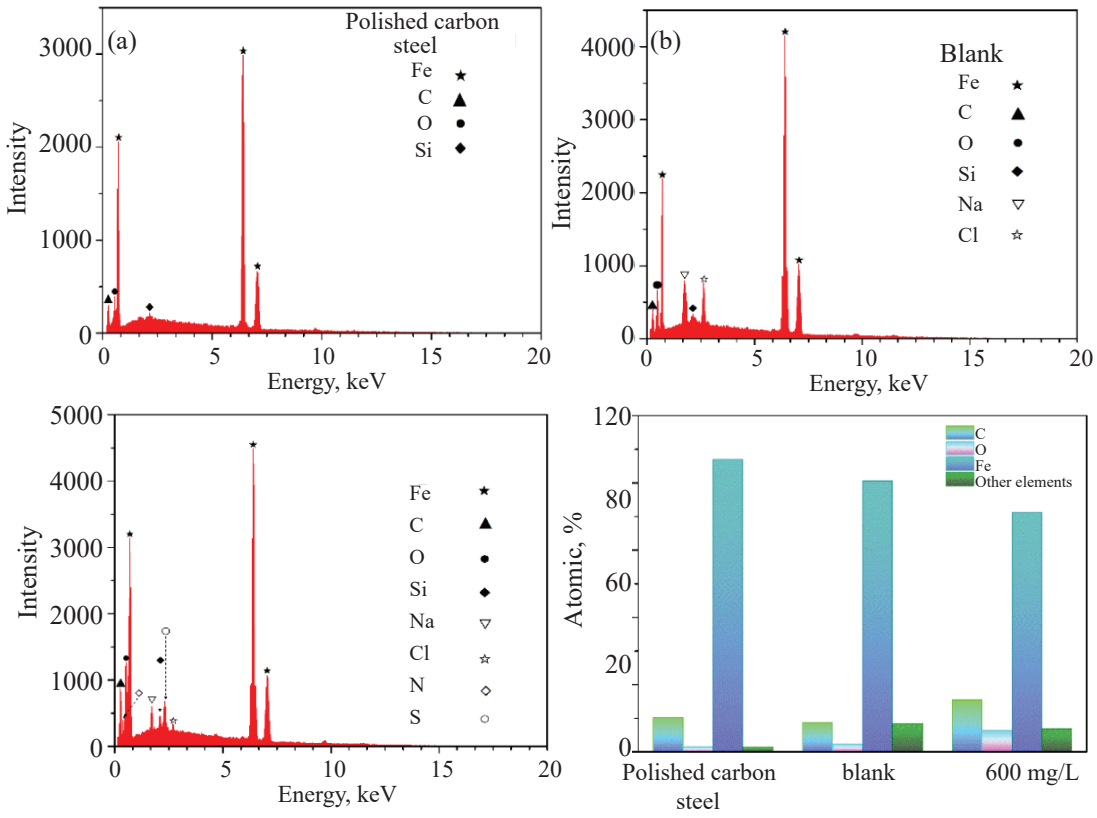

Fig. 15. (Color online) The EDS spectra for the N80 carbon steel after 72 h of immersion in saturated CO_2 3% NaCl solution without and with 600 mg/L N-CQDs.

atomic content of Fe and C for polished N80 carbon steel is 87.01% and 10.22%, and those for N80 carbon steel immersion in saturated-CO_2 3% NaCl solution absence and presence of 600 mg/L N-CQDs are 80.66%, 8.67%, and 71.27%, 15.48%, respectively. The fact that relative content of oxygen increases more, while that of iron decreases more, is attributed to the formation of inhibitor protective layer on N80 carbon steel by N-CQDs.

CONCLUSION

Novel disodium ethylenediamine tetraacetate-based carbon dots containing amino sulfonic acid and urotropine were synthesized, the corrosion of N80 carbon steel in saturated CO_2 3 wt % NaCl solution can be prevented effectively by adding N-CQDs, and with the increases of N-CQDs, the corrosion inhibition effect becomes more obvious. The main conclusions are as follows:

–The particle size of N-CQDs are 4–8 nm with good dispersion performance;

– N-CQDs are amorphous solid structure and have strong hydrophilicity;

– N-CQDs can effectively protect carbon steel from corrosion, with inhibition efficiency reaching 83.7% at 600 mg/L;

– The electrochemical results show that the lone pair electrons in N-CQDs can coordinate with the iron-air orbits to adsorb on the surface of carbon steel, effectively increase the charge transfer resistance, reduce the double-layer capacitance and film capacitance, and inhibit the corrosion of N80 steel;

– SEM and EDS characterization revealed that N, S elements appeared on the surface of carbon steel, indicating that N-CQDs can be adsorbed on the surface of carbon steel.

ACKNOWLEDGMENTS

The authors thank the Southwest Petroleum University, Institute, Chengdu, China and the Scientific Compass Test Platform for providing the research facilities needed for the above study. This work was supported by the National Science

and Technology Major Project of China (no. 2016ZX05016-004-008).

CONFLICT OF INTEREST

The authors declare no conflict of interest.

REFERENCE

1. Baddoo, N.R., *J. Construct. Steel Res.,* 2008, vol. 64, no. 11, pp. 1199–1206. https://doi.org/10.1016/j.jcsr.2008.07.011
2. Malik, A.U., Kutty, P.C.M., Andijani, I.N., et al., *Desalination,* 1994, vol. 97, nos. 1–3, pp. 171–187. https://doi.org/10.1016/0011-9164(94)00085-9
3. Gurrappa, I., *J. Materials Processing Technology,* 2005, vol. 166, no. 2, pp. 256–267. https://doi.org/10.1016/j.jmatprotec.2004.09.074
4. Hua, Y., Barker, R., and Neville, A., *J. Supercritical Fluids,* 2015, vol. 97, pp. 224–237. https://doi.org/10.1016/j.supflu.2014.12.005
5. Xiang, Y., Long, Z., Li, C., et al., *Int. J. Greenhouse Gas Control,* 2017, vol. 63, pp. 141–149. https://doi.org/10.1016/j.ijggc.2017.05.010
6. Laumb, J.D., Glazewski, K.A., Hamling, J.A., et al., *Energy Procedia,* 2017, vol. 114, pp. 5173–5181. https://doi.org/10.1016/j.egypro.2017.03.1671
7. Zhang, Y., Pang, X., Qu, S., et al., *Corrosion Sci.,* 2012, vol. 59, pp. 186–197. https://doi.org/10.1016/j.corsci.2012.03.006
8. Gao, M., Pang, X., and Gao, K., *Corrosion Sci.,* 2011, vol. 53, no. 2, pp. 557–568. https://doi.org/10.1016/j.corsci.2010.09.060
9. Ezuber, H.M., *Materials and Design,* 2009, vol. 30, no. 9, pp. 3420–3427. https://doi.org/10.1016/j.matdes.2009.03.028
10. Foley, R.T., *Corrosion,* 1970, vol. 26, no. 2, pp. 58–70. https://doi.org/10.5006/0010-9312-26.2.58
11. Pandarinathan, V., Lepková, K., Bailey, S.I., et al., *Corrosion Sci.,* 2013, vol. 72, pp. 108–117. https://doi.org/10.1016/j.corsci.2013.03.013
12. Obot, I.B. and Obi-Egbedi, N.O., *Corrosion Sci.,* 2010, vol. 52, no. 1, pp. 198–204. https://doi.org/10.1016/j.corsci.2009.09.002
13. Askari, M., Aliofkhazraei, M., Ghaffari, S., et al., *J. Natural Gas Sci. and Eng.,* 2018, vol. 58, pp. 92–114. https://doi.org/10.1016/j.jngse.2018.07.025
14. Zhou, J., Zhou, H., Tang, J., et al., *Microchimica Acta,* 2017, vol. 184, no. 2, pp. 343–368. https://doi.org/10.1007/s00604-016-2043-9
15. Ramanan, V., Thiyagarajan, S.K., Raji, K., et al., *ACS Sustainable Chem. & Eng.,* 2016, vol. 4, no. 9, pp. 4724–4731. https://doi.org/10.1021/acssuschemeng.6b00935
16. Xu, Q., Kuang, T., Liu, Y., et al., *J. Mat. Chem. B,* 2016, vol. 4, no. 45, pp. 7204–7219. https://doi.org/10.1039/C6TB02131J
17. Yuan, F., Li, S., Fan, Z., et al., *Nano Today,* 2016, vol. 11, no. 5, pp. 565–586. https://doi.org/10.1016/j.nantod.2016.08.006
18. Wang, Q., Zheng, H., Long, Y., et al., *Carbon,* 2011, vol. 49, no. 9, pp. 3134–3140. https://doi.org/10.1016/j.carbon.2011.03.041
19. Kumar, A., Chowdhuri, A.R., Laha, D., et al., *Sensors & Actuators B: Chem.,* 2017, vol. 242, pp. 679–686. https://doi.org/10.1016/j.snb.2016.11.109
20. Li, Y., Zhao, Y., Cheng, H., et al., *J. Am. Chem. Soc.,* 2011, vol. 134, no. 1, pp. 15–18. https://doi.org/10.1021/ja206030c
21. Shen, J., Zhang, T., Cai, Y., et al., *New J. Chemistry,* 2017, vol. 41, no. 19, pp. 11125–11137. https://doi.org/10.1039/C7NJ00505A
22. Liu, T., Cui, Z., Zhou, J., et al., *Nanoscale Res. Lett.,* 2017, vol. 12, no. 1, p. 375. https://doi.org/doi:10.1186/s11671-017-2149-y
23. Dang, D.K., Sundaram, C., Ngo, Y.L.T., et al., *Sensors and Actuators B: Chem.,* 2018, 255, pp. 3284–3291. https://doi.org/10.1016/j.snb.2017.09.155
24. Zhang, H., Chen, Y., Liang, M., et al., *Anal. Chem.,* 2014, vol. 86, no. 19, pp. 9846–9852. https://doi.org/10.1021/ac502446m
25. Cen, H., Chen, Z., and Guo, X., *J. Taiwan Institute Chem. Eng.,* 2019, vol. 99, pp. 224–238. https://doi.org/10.1016/j.jtice.2019.02.036
26. Yang, Q., Duan, J., Yang, W., et al., *Appl. Sur. Sci.,* 2018, vol. 434, pp. 1079–1085. https://doi.org/10.1016/j.apsusc.2017.11.040
27. Das, S., Kumar, S., Samal, S.K., et al., *Industrial & Engineering Chemistry Res.,* 2018, vol. 57, no. 8, pp. 2727–2745. https://doi.org/10.1016/j.apsusc.2016.04.186
28. Darmanin, T., de Givenchy, E.T., Amigoni, S., et al., *Adv. Materials,* 2013, vol. 25, no. 10, pp. 1378–1394. https://doi.org/10.1002/adma.201204300
29. Choi, B.G., Park, H.S., *J. Phys. Chem. C,* 2012, vol. 116, no. 5, pp. 3207–3211. https://doi.org/10.1021/jp207818b
30. Cui, M., Ren, S., Xue, Q., et al., *J. Alloys and Compounds,* 2017, vol. 726, pp. 680–692. https://doi.org/10.1016/j.jallcom.2017.08.027
31. Cui, M., Ren, S., Zhao, H., et al., *Appl. Sur. Sci.,* 2018,

vol. 443, pp. 145–156.
https://doi.org/10.1016/j.apsusc.2018.02.255

32. Tourabi, M., Nohair, K., Traisnel, M., et al., *Corrosion Sci.,* 2013, vol. 75, pp. 123–133.
https://doi.org/10.1016/j.corsci.2013.05.023
33. Sığırcık, G., Tüken, T., and Erbil, M., *Appl. Sur. Sci.,* 2015, vol. 324, pp. 232–239.
https://doi.org/10.1016/j.apsusc.2014.09.206
34. Bayol, E., Gürten, A, A., Dursun, M., et al., *Acta Physico-Chimica Sinica,* 2008, vol. 24, no. 12, pp. 2236–2243.
https://doi.org/10.1016/S1872-1508(08)60085-6
35. Avci, G., *Materials Chemistry and Physics,* 2008, vol. 112, no. 1, pp. 234–238.
https://doi.org/10.1016/j.matchemphys.2008.05.036
36. Oguzie, E.E., *Materials Chemistry and Physics,* 2006, vol. 99, nos. 2–3, pp. 441–446.
https://doi.org/10.1016/j.matchemphys.2005.11.018
37. Solmaz, R., *Corrosion Sci.,* 2014, vol. 79, pp. 169–176.
https://doi.org/10.1016/j.corsci.2013.11.001
38. Bentiss, F., Traisnel, M., and Lagrenee, M., *Corrosion Sci.,* 2000, vol. 42, no. 1, pp. 127–146.
https://doi.org/10.1016/S0010-938X(99)00049-9
39. Obot, I.B., Umoren, S.A., Gasem, Z.M., et al., *Ind. & Eng. Chem. Res.,* 2015, vol. 21, pp. 1328–1339.
https://doi.org/10.1016/j.jiec.2014.05.049
40. Hegazy, M.A., *Corrosion Sci.,* 2009, vol. 51, no. 11, pp. 2610–2618.
https://doi.org/10.1016/j.corsci.2009.06.046
41. Bedair, M.A., El-Sabbah, M.M.B., Fouda, A.S., et al., *Corrosion Sci.,* 2017, vol. 128, pp. 54–72.
https://doi.org/10.1016/j.corsci.2017.09.016
42. Mourya, P., Banerjee, S., and Singh, M.M., *Corrosion Sci.,* 2014, vol. 85, pp. 352–363.
https://doi.org/10.1016/j.corsci.2014.04.036
43. Lebrini, M., Lagrenée, M., Vezin, H., et al., *Corrosion Sci.,* 2007, vol. 49, no. 5, pp. 2254 –2269.
https://doi.org/10.1016/j.corsci.2006.10.029
44. Zhao, J. and Chen, G., *Electrochimica Acta,* 2012, vol. 69, pp. 247–255.
https://doi.org/10.1016/j.electacta.2012.02.101
45. Li, P., Lin, J.Y., Tan, K.L., et al., *Electrochimica Acta,* 1997, vol. 42, no. 4, pp. 605–615.
https://doi.org/10.1016/S0013-4686(96)00205-8
46. Murulana, L.C., Singh, A.K., Shukla, S.K., et al., *Ind. & Eng. Chem. Res.,* 2012, vol. 51, no. 40, pp. 13282–13299.
https://doi.org/10.1021/ie300977d
47. Bergel, A., Féron, D., and Mollica, A., *Electrochem. Comm.,* 2005, vol. 7, no. 9, pp. 900–904.
https://doi.org/10.1016/j.elecom.2005.06.006
48. Zhang, S., Tao, Z., Liao, S., et al., *Corrosion Sci.,* 2010, vol. 52, no. 9, pp. 3126–3132.
https://doi.org/10.1016/j.corsci.2010.05.035